J. Fluid Mech. (1994), *vol.* 268, *pp.* 71–88

Temporal stability of Jeffery–Hamel flow

By MAHMOUD HAMADICHE, JULIAN SCOTT AND DENIS JEANDEL

Laboratoire de Mécanique des Fluides et d'Acoustique, Ecole Centrale de Lyon, 36, avenue Guy-de-Collongue, BP 163, 69131 Ecully, France

(Received 5 February 1992 and in revised form 4 October 1993)

In this study of the temporal stability of Jeffery–Hamel flow, the critical Reynolds number based on the volume flux, R_c, and that based on the axial velocity, Re_c, are computed. It is found that both critical Reynolds numbers decrease very rapidly when the half-angle of the channel, α, increases, such that the quantity αR_c remains very nearly constant and αRe_c is a nearly linear function of α. For a short channel there can be more than one value of the critical Reynolds number. A fully nonlinear analysis, for Re close to the critical value, indicates that the loss of stability is supercritical. The resulting asymmetric oscillatory solutions show staggered arrays of vortices positioned along the channel.

1. Introduction

The steady two-dimensional flow of viscous, incompressible fluid within an infinite wedge driven by a line source situated at the intersection of the rigid planes that form the wedge is termed Jeffery–Hamel flow. The nonlinear governing equation, first given by Jeffery (1915) and Hamel (1916), was solved by Fraenkel (1962*a*, *b*). Two types of solution were found, namely those which are symmetric under reflection in the centreplane of the wedge and those which are asymmetric with respect to such reflection. This paper is solely concerned with the symmetric solution, which depends upon two non-dimensional parameters: α, the wedge semi-angle; and $R = Q/2\nu$, the Reynolds number based on the volume flux, Q. Different regions of the (α, R)-plane were classified by Fraenkel in terms of the number of zeros of the solution. The regions which we consider were denoted I, II_1, and II_2 by Fraenkel, and we shall see that they include the critical Reynolds number for temporal instability.

Following Dean (1934), Banks, Drazin & Zaturska (1988) considered a perturbation of Jeffery–Hamel flow independent of time and having the form r^λ, where (r, θ) are cylindrical polar coordinates with axis at the wedge apex. They solve for λ as a function of α and R and find that $\lambda = 0$ leads to the curve B_2 defined by Fraenkel as the boundary between regions II_1 and II_2. They interpret this as giving the neutral curve for spatial stability. As noted by these authors, this interpretation is not more than plausible since the existence of a mode which grows at $r = 0$ or at $r = \infty$ is no guarantee of spatial instability; indeed if this were the case the results indicate spatial instability for any values of α and R. To clarify this point, an initial-value problem in which a time-harmonic source of perturbations is switched on at $t = 0$ and persists to $t = \infty$ should be solved with appropriate boundary conditions at $r = 0$ and $r = \infty$. One could then observe if the solution approaches large values as $t \to \infty$. Lack of such an analysis led Bramley & Dennis (1982) to the incorrect conclusion that the critical Reynolds number for spatial instability of plane Poiseuille flow is $Re = 5$, where Re is the Reynolds number based on the centreplane velocity ($R = \frac{2}{3}Re$ for plane Poiseuille

flow). In fact, spatial instability of plane flows requires that they be temporally unstable, i.e. $Re > 5772$ in the case of Poiseuille flow. The 'growing' modes which they found instead represent evanescent solutions decaying away from a source of perturbations.

Eagles (1966) investigated the temporal stability of Jeffery–Hamel flow using a number of approximations which he claims are valid in the limit $\alpha \to 0$. Using these approximations, the plane Orr–Sommerfeld equation is obtained, but with a velocity profile different from plane Poiseuille flow. The resulting critical Reynolds numbers are typically much less than the classical Poiseuille value, $Re = 5772$, and we obtain such low values also. We shall compare our result to those of Eagles later and, paradoxically, find poor agreement when α is small, but reasonable agreement for larger values of α.

Another approximate method was used by Sobey & Drazin (1986) to study temporal instability of the flow. This was based on linearization of a heuristic dynamical model due to Hooper, Duffy & Moffatt (1982). Sobey & Drazin find that the resulting neutral curve is B_2. Despite the approximations implicit in the work of Sobey & Drazin, our exact analysis is in good agreement with their results. In the same paper Sobey & Drazin also describe an interesting result for a class of different channel flows using full numerical Navier–Stokes simulation and experimental visualization.

In this paper we treat the exact linear temporal instability of the flow in a finite domain $r_1 < r < r_2$ subject to a two-dimensional perturbation. Banks *et al.* (1988) studied the same problem when $R = 0$ and found, not surprisingly, that the flow is stable. Furthermore, for $R = 0$ in the limit $\alpha \to 0$ and $r_1/r_2 \to 1$ they show that the smallest non-dimensional temporal decay rate approaches $(\pi/\alpha)^2$. We shall later compare our results with this value.

The channel flow described by the Jeffery–Hamel solution is usually considered infinite in streamwise extent. From a numerical point of view, this creates difficulties. Also the boundary conditions to be applied at $r = 0$ and at $r = \infty$ are unknown *a priori*. To get around these problems we consider a finite portion of the channel, $r_1 < r < r_2$, and impose somewhat arbitrary boundary conditions on the perturbation at $r = r_1$ and $r = r_2$ (see §3 for details). We find that the results converge as $r_2/r_1 \to \infty$ and we interpret the limiting values as appropriate to an infinite channel.

When α goes to zero we might expect the result to approach those for plane Poiseuille flow. The stability of that flow has been widely studied. Lin (1945*a*, *b*) used an analytical method to find the neutral curve in the (k_1, Re)-plane, where k_1 is the streamwise wavenumber. Thomas (1953) confirmed Lin's results using a finite difference method. Later these results were refined by other researchers using more accurate and efficient methods, such as Grosch & Salwen (1968) who proposed a spectral method using trial functions which comply with boundary conditions, Orszag (1971) who expanded the solution in Chebyshev polynomial series, and Mele *et al.* (1981) who used a finite element method. These authors show that the critical Reynolds number is $Re_c = 5772$. In order that Jeffery–Hamel flow approaches plane Poiseuille flow, we require $\alpha Re \to 0$ and $\alpha \to 0$. At the critical value Re_c we therefore need $\alpha \ll (Re_c)^{-1}$ and such small values of α lead to numerical problems with the methods used in this paper. For this reason no comparisons with plane Poiseuille flow were possible and we do not discuss this issue further. It is worth emphasizing that the values of Re_c that we find in the range of α considered are much lower than those for plane Poiseuille flow.

Jeffery–Hamel flow and the linear equation governing a small disturbance of the usual form e^{st}, where s is the complex growth rate, are introduced in §2. The special case of steady modes (i.e. $s = 0$) of the form r^λ is also discussed. The numerical method

used to solve the linear equation for a small unsteady disturbance is presented in §3. The main objective is to compute the critical Reynolds number: the linear equation is solved using an expansion in trial functions which complies with the boundary conditions, leading to an algebraic eigenvalue problem which is solved using the 'QZ' method. Section 4 contains the result of the linear analysis and a comparison with Eagles' (1966) method and the Hooper *et al.* (1982) model.

In §5, the nonlinear behaviour of the flow perturbation is considered using an expansion in the linear eigenfunctions, projection onto the adjoint eigenfunction and truncation. The interaction between stable and unstable modes is discussed. For Reynolds numbers above the critical value, time-periodic and quasi-periodic solutions occur. For Reynolds numbers below critical, we find that the perturbation died away in all cases we computed. This suggest that, unlike plane Poiseuille flow, Jeffery–Hamel flow is supercritical unless the value of α is very small (smaller than those considered here). Finally plots of the stream functions of the nonlinear solution are given.

2. Basic equations

Let ψ be the stream function of two-dimensional flow of an incompressible fluid of kinematic viscosity ν. In terms of ψ, the vorticity equation is

$$\nu\nabla^4\psi+\frac{1}{r}\frac{\partial(\psi,\nabla^2\psi)}{\partial(r,\theta)}=\frac{\partial(\nabla^2\psi)}{\partial t}, \tag{2.1}$$

where cylindrical polar coordinates (r,θ) are used. We introduce dimensionless scaled variables, $y=\theta/\alpha$, $\rho=r/r_2$ and $\tau=\nu t/r_2^2$, where α is the semi-angle of the channel, t is time and r_2 is a distance which is arbitrary at this stage, but will be specified later as the outer radius of the flow domain.

2.1. *Jeffery–Hamel flow*

The basic flow is driven by a given steady volume flux Q between two rigid walls, $\theta=\pm\alpha$. The boundary conditions of no slip and impermeability are

$$\psi=\pm\tfrac{1}{2}Q, \quad \psi_\theta=0 \quad \text{at} \quad \theta=\pm\alpha. \tag{2.2}$$

We write $\psi=\frac{1}{2}QG(y)$, and $R=Q/2\nu$ as the Reynolds number based on the flux. Equation (2.1) with the boundary conditions (2.2) becomes

$$G_{yyyy}+4\alpha^2G_{yy}+2\alpha RG_yG_{yy}=0, \tag{2.3}$$

$$G=\pm1, \quad G_y=0 \quad \text{at} \quad y=\pm1. \tag{2.4}$$

The flow described by the system (2.3) and (2.4) is Jeffery–Hamel flow and has been classified by Fraenkel (1962*a*, *b*) into types I, II_n, III_n, IV_n, V_n. We will focus attention on the stability of the flow in the regions of parameter space denoted by I, II_1, and II_2. The solutions of the system (2.3) and (2.4) are also discussed by Hooper *et al.* (1982) using a numerical method which, in our view, is easier to follow than the elliptic functions of Fraenkel (1962*a*, *b*).

2.2. *The linear equation for the perturbation*

Taking the Jeffery–Hamel solution as the basic flow, we substitute $\psi=\frac{1}{2}Q(G+\psi')$ into (2.1) and neglect nonlinear terms in ψ'; we find

$$\frac{\partial(\nabla^2\psi')}{\partial\tau}+\frac{RG_y}{\alpha\rho}\frac{\partial(\nabla^2\psi')}{\partial\rho}-\frac{2RG_{yy}}{\alpha^3\rho^4}\frac{\partial\psi'}{\partial y}-\frac{RG_{yyy}}{\alpha^3\rho^3}\frac{\partial\psi'}{\partial\rho}=\nabla^4\psi', \tag{2.5}$$

with

$$\psi'=0, \quad \psi'_y=0 \quad \text{at} \quad y=\pm1. \tag{2.6}$$

To complete the system, there should also be boundary conditions at $r = 0$ and $r = \infty$ in the case of an infinite channel and at $r = r_1$ and $r = r_2$ for the finite channel. The precise boundary conditions for an infinite channel are not obvious, and we state those for a finite channel in §3.

2.3. *Temporal instability*

Unsteady normal modes may be taken of the form $\psi' = \exp(s\tau)\,\Phi(\rho, y)$. Equations (2.5) and (2.6) become

$$s\nabla^2\Phi + \frac{RG_y}{\alpha\rho}\frac{\partial(\nabla^2\Phi)}{\partial\rho} - \frac{2RG_{yy}}{\alpha^3\rho^4}\frac{\partial\Phi}{\partial y} - \frac{RG_{yyy}}{\alpha^3\rho^3}\frac{\partial\Phi}{\partial\rho} = \nabla^4\Phi, \tag{2.7}$$

with

$$\Phi = 0, \quad \Phi_y = 0 \quad \text{at} \quad y = \pm 1. \tag{2.8}$$

As usual the flow is judged temporally unstable if one or more of the possible values of s have positive real parts.

2.4. *Steady solutions*

Following Dean (1934), steady normal modes ($s = 0$) of the form $\psi' = \rho^{\lambda}\hat{\psi}(y)$ can be found. Equations (2.5) and (2.6) become

$$\hat{\psi}_{yyyy} + \alpha^2(\lambda^2 + (\lambda-2)^2)\,\hat{\psi}_{yy} + \alpha^4\lambda^2(\lambda-2)^2\hat{\psi} - \alpha R(\lambda-2)\,G_y(\hat{\psi}_{yy} + \alpha^2\lambda^2\hat{\psi}) + \alpha R\lambda G_{yyy}\hat{\psi} + 2\alpha G_{yy}\hat{\psi}_y = 0. \tag{2.9}$$

with

$$\psi' = 0, \quad \psi'_y = 0 \quad \text{at} \quad y = \pm 1. \tag{2.10}$$

Banks *et al.* (1988) used both numerical and analytical methods to solve the system (2.9), (2.10) and interpreted their results as showing that the curve B_2 (which was introduced by Fraenkel 1962*a*, *b* as the boundary between domains II_1 and II_2) gives the onset of spatial stability. We have expressed our reservation as to this interpretation in the introduction.

3. Numerical method

As stated in §2.2, the unique boundary conditions applied at $r = 0$ and $r = \infty$ for an infinite channel are not obvious and for this reason, and for the sake of numerical simplicity, we introduce a finite channel, $r_1 < r < r_2$. Using the scaled non-dimensional coordinates introduced previously the channel occupies $-1 < y < 1$, $\rho_1 < \rho < 1$, where $\rho_1 = r_1/r_2$. We introduce the dimensionless parameter $\Delta = 1 - \rho_1$, which represents the length of the channel ($0 < \Delta < 1$).

Let F be the function $F(y) = G_y(y)/G_y(0)$ and $Re = r\alpha U_0/\nu$ the Reynolds number based on the centreplane velocity U_0 which, according to Batchelor (1977, p. 295), gives a more direct measure of the intensity of the flow than R. For a symmetric solution of Jeffery–Hamel flow, (2.3) and (2.4) become

$$F_{yyy} + 4\alpha^2 F_y + 2\alpha ReFF_y = 0, \tag{3.1}$$

with

$$F_y = 0 \quad \text{at} \quad y = 0, \tag{3.2}$$

$$F = 1 \quad \text{at} \quad y = 0, \tag{3.3}$$

$$F = 0 \quad \text{at} \quad y = -1. \tag{3.4}$$

In terms of the function F, we can easily obtain a relationship between the two Reynolds numbers R and Re defined previously:

$$R = \tfrac{1}{2}Re\int_{-1}^{+1} F(y)\,\mathrm{d}y. \tag{3.5}$$

To obtain the function $F(y)$ we solve the first integral of (3.1) (for which the constant

of integration can be obtained in terms of $F_y(-1)$ using (3.2)–(3.4)) numerically using fourth-order Runge–Kutta and the 'shooting' method. This provides the basic flow by iteration, starting from (3.4) and an estimate of $F_y(-1)$. The estimate was obtained as follows. For $Re = 0$ the solution is known analytically and, with $\alpha = 0.1$, we varied αRe in small increments away from zero to cover the interval $0 < \alpha Re < 45$, iterating at each stage. For values of $\alpha < 0.5$ rad and Re different from those computed but whose product is in the given range, we obtained the initial $F_y(-1)$ by forming the product αRe and using the value appropriate to the nearest of the computed αRe. Newton–Raphson iteration was then used to determine the true value of $F_y(-1)$. In all cases the iteration converged rapidly when αRe was in the given interval.

Using F, (2.7) and (2.8) for the perturbation become

$$s\nabla^2\Phi + \frac{ReF}{\alpha\rho}\frac{\partial(\nabla^2\Phi)}{\partial\rho} - \frac{2ReF_y}{\alpha^3\rho^4}\frac{\partial\Phi}{\partial y} - \frac{ReF_{yy}}{\alpha^3\rho^3}\frac{\partial\Phi}{\partial\rho} = \nabla^4\Phi, \tag{3.6}$$

with

$$\Phi = 0, \quad \Phi_y = 0 \quad \text{at} \quad y = \pm 1. \tag{3.7}$$

As discussed in §2.2 we need boundary conditions at $r = r_1$ and $r = r_2$ to complete the problem. Two distinct types of somewhat arbitrary conditions are used. The first are the simplest conditions, namely

$$\Phi_\rho = \Phi = 0 \quad \text{at} \quad \rho = \rho_1, \tag{3.8}$$

with

$$\Phi_\rho = \Phi = 0 \quad \text{at} \quad \rho = 1, \tag{3.9}$$

and will be referred as zcro boundary conditions. The second are

$$\Phi(\rho_1) = \Phi(1), \tag{3.10}$$

$$\Phi_\rho(\rho_1) = \Phi_\rho(1), \tag{3.11}$$

and will be called 'periodic' boundary conditions (of course, the solution outside the range $\rho_1 < \rho < 1$ would not be periodic). Later we will see that the results converge as $r_2/r_1 \to \infty$, i.e. $\Delta \to 1$, and become dependent only on the parameters α and R.

The function Φ is expanded as a linear combination of basis functions which comply with the boundary conditions. Because the basic flow is symmetric under reflection in $y = 0$ the eigenfunction, Φ, is either symmetric or antisymmetric in y. The symmetric solutions have the form

$$\Phi = \sum_{i=1}^{M} X_i(y)\left(\sum_{j=1}^{N_1} a_{ij} P_j(\rho) + \sum_{j=1}^{N_2} b_{ij} Q_j(\rho)\right), \tag{3.12}$$

while the antisymmetric functions are

$$\Phi = \sum_{i=1}^{M} Y_i(y)\left(\sum_{j=1}^{N_1} a_{ij} P_j(\rho) + \sum_{j=1}^{N_2} b_{ij} Q_j(\rho)\right). \tag{3.13}$$

Following Hamadiche (1985) the basis functions X_i, Y_i are particular solutions of the Orr–Sommerfeld equation for plane Poiseuille flow when the wavenumber in the streamwise direction is zero; they are given by

$$X_i(y) = \frac{\cosh(qy)}{\cosh(q)} - \frac{\cos(\gamma_i y)}{\cos(\gamma_i)} \tag{3.14}$$

and

$$Y_i(y) = \frac{\sinh(qy)}{\sinh(q)} - \frac{\sin(\beta_i y)}{\sin(\beta_i)}. \tag{3.15}$$

Here γ_i, β_i are respectively the real positive solutions of the equations

$$q\tanh(q) + \gamma_i \tan(\gamma_i) = 0 \tag{3.16}$$

and $$q\coth(q)-\beta_i\cot(\beta_i)=0 \tag{3.17}$$

and q is an arbitrary real constant which we take equal to 2. The functions X_i, Y_i are used simply because they form a convenient complete set on the interval $-1<y<1$, such that they and their first derivatives are zero at the end points $y=\pm 1$.

The basis function P_j and Q_j depend upon the type of boundary conditions used. When the zero boundary conditions (3.8) and (3.9) are employed we take

$$P_j(\rho)=X_j(x(\rho)) \tag{3.18}$$

and $$Q_j(\rho)=Y_j(x(\rho)), \tag{3.19}$$

where $$x(\rho)=\frac{2\rho-(1+\rho_1)}{1-\rho_1}. \tag{3.20}$$

For the second type of boundary condition

$$P_j(\rho)=\cos(j\pi x(\rho)) \tag{3.21}$$

and $$Q_j(\rho)=\sin(j\pi x(\rho)). \tag{3.22}$$

The expansion for Φ is introduced into (3.6), the result is multiplied by either $X_i(y)$ or $Y_i(y)$, depending upon the symmetry of Φ, and the result is integrated over y; further multiplication by either $P_j(\rho)$ or $Q_j(\rho)$ and integration over ρ yields a set of linear equations of the form $$s\Xi\xi=\Lambda\xi \tag{3.23}$$

for the coefficients a_{ij} and b_{ij} represented by the column vector ξ. The eigenvalues and eigenfunctions of the above system are obtained by the 'QZ method.

When we come to discuss the nonlinear stability problem we will need the adjoint linear eigenfunctions. These are determined by the solutions of the adjoint eigenvalue problem: $$s\Xi^T\xi^A=\Lambda^T\xi^A \tag{3.24}$$

which has the same eigenvalues as (3.23). Here Ξ^T represents a matrix transpose and ξ^A is the vector of coefficients of the adjoint eigenfunction with the same basis functions as before.

According to Banks *et al.* (1988), s is real and negative when the Reynolds number is zero. We denote the largest value of the real part of s by s_g. The range of Reynolds numbers which we wanted to cover was subdivided into a large number of segments and interval halving on each segment used to find any zeros of s_g. This procedure gives the value (or values) of Re_c.

4. Results and discussion

4.1. *The case* $Re=0$

When the Reynolds number is taken equal to zero, the linear stability problem does not contain the basic flow, as can be seen from (3.6). Banks *et al.* (1988) proved that when $Re=0$ and both α and Δ go to zero, s_g tends to $-(\pi/\alpha)^2$. Below, we compare this limit with our numerical evaluation of s_g, using zero boundary conditions.

With $\alpha=10^{-4}$, and $\rho_1=0.99$ Banks *et al.* found that $\alpha^2 s_g=-9.96$ by numerical integration. Our result, using zero boundary conditions, is identical, see table 1.

4.2. *Comparison with Hooper et al.'s model*

Rather than the exact linear problem (3.6), (3.7), Hooper *et al.* (1982), and Sobey & Drazin (1986) considered a nonlinear model, namely

$$G_{yyt}=G_{yyyy}+4\alpha^2G_{yy}+2\alpha RG_yG_{yy} \tag{4.1}$$

with $$G\pm 1,\quad G_y=0\quad \text{at}\quad y=\pm 1. \tag{4.2}$$

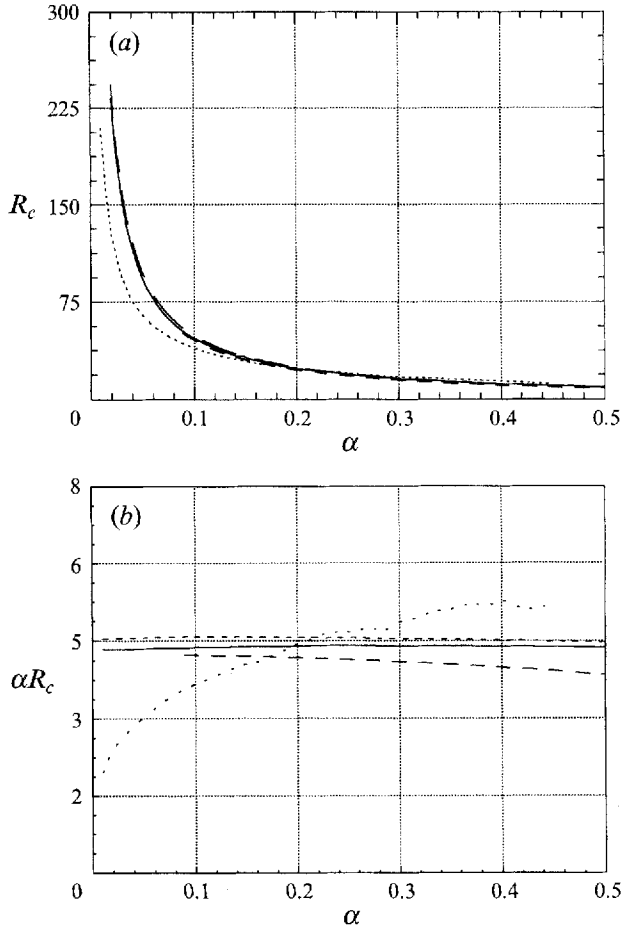

FIGURE 1. (*a*) A plot of the critical Reynolds number R_c, based on the volume flux, against the half-angle of the channel, α: ——, the present method using zero boundary conditions; – – –, the present method using periodic boundary conditions; ·····, Eagles; ----, Sobey & Drazin using Hooper *et al.*'s model. $\Delta = 0.999$ in calculations using the present method. (*b*) As (*a*) but showing αR_c instead of R_c: ——, the present method using zero boundary conditions; ----, the present method using periodic boundary conditions; ·····, Eagles; – – –, Sobey & Drazin using Hopper *et al.*'s model.

α	0.2	0.1	0.01	0.001	0.0001
$\alpha^2 s_g$	−15149	−3722	−39.13	−9.52	−9.96

TABLE 1. Numerical evaluation of $\alpha^2 s_g$. According to Banks *et al.* (1988) the limit is $-\pi^2$ when $\alpha \to 0$, $\Delta \to 1$.

Among other results, Sobey & Drazin (1986) showed that if (4.1) is linearized using Jeffery–Hamel as the basic flow, it results in the curve B_2 for the temporal neutral curve. In figure 1 (*a*) we compare this result with the neutral curve given by the present method. The results are in surprisingly good agreement.

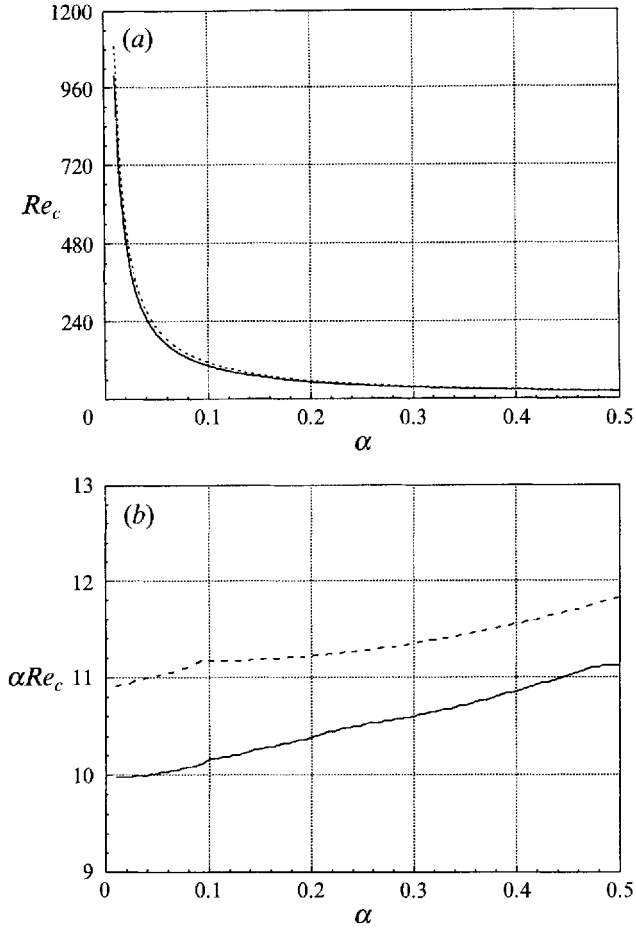

FIGURE 2. (*a*) The critical Reynolds number Re_c based on axial velocity as given by the present method: ——, zero boundary conditions; ····· periodic boundary conditions. $\Lambda = 0.999$ in both cases. (*b*) As (*a*) but showing αRe_c instead of Re_c.

4.3. *Main results*

In figure 1(*a*) we compare the critical Reynolds numbers based on the volume flux obtained by Eagles (1966) and given by the present method using 12 trial functions in each direction. The results shown are for $\Lambda = 0.999$, corresponding to a long channel, as an approximation of Eagles' unbounded channel. Note that the results are in agreement for the larger values of α ($\alpha > 0.15$ rad), while for small values of α ($\alpha < 0.15$ rad) our method, using both zero and periodic boundary conditions, predicts a higher critical Reynolds number; this may be because, in spite of the fact that Eagles' approximation is supposedly valid only when α is small, the argument of the exponential term in equation (5) of his paper may go to infinity in an unbounded domain even for small α, and cannot then be neglected.

In figure 1(*b*) we plot the same data shown in figure 1(*a*) in the plane (αR_c, α). Both our results and those given by the model of Hooper *et al.* show that the product αR_c is very nearly a linear function of α, while Eagles' results are in disagreement.

Figure 2(*a*) shows the critical Reynolds number based on the axial velocity Re_c for both zero and periodic boundary conditions and $\Lambda = 0.999$. The critical Reynolds number decreases rapidly with increasing α. Note that the corresponding neutral mode

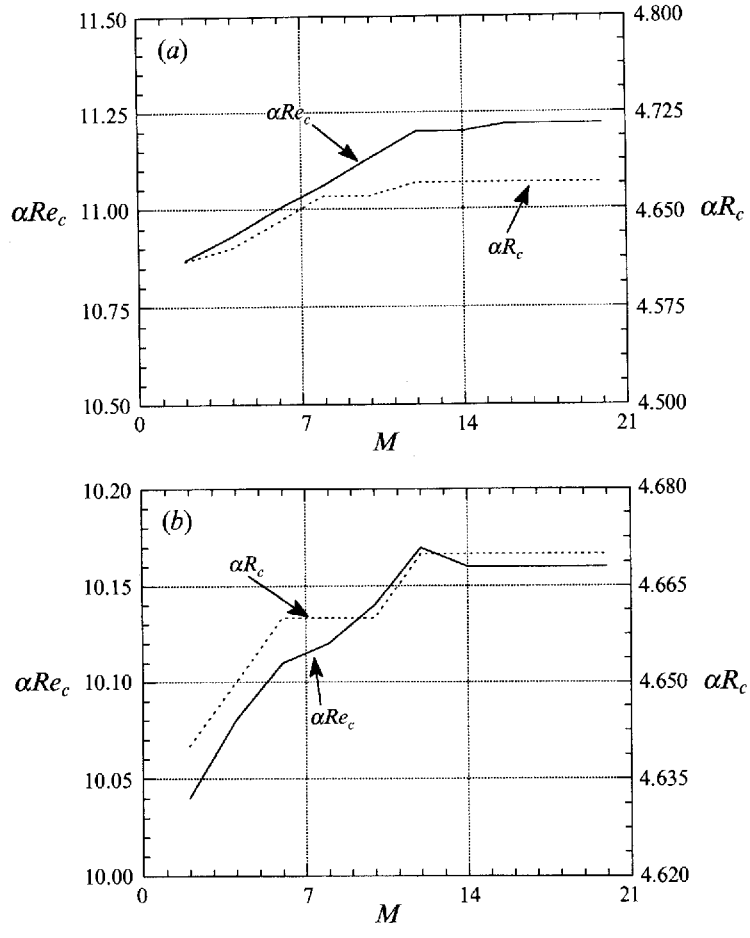

FIGURE 3. The critical Reynolds number obtained using different numbers of trial functions M ($N_1 = N_2 = \frac{1}{2}M$). Re_c is the critical Reynolds number based on the axial velocity, R_c the critical Reynolds number based on the volume flux. Zero boundary conditions and $\Delta = 0.999$. (*a*) $\alpha = 0.5$, (*b*) $\alpha = 0.1$.

is symmetric with respect to y. The difference between the critical Reynolds number obtained using zero and periodic boundary conditions is small but greater than the numerical error and becomes more apparent in the (αRe_c, α)-plane (see figure 2*b*). The difference between the two critical Reynolds numbers is about 10%.

In figures 3(*a*) and 3(*b*) we plot the critical Reynolds number using different numbers ($M = 2N_1 = 2N_2$) of trial functions for $\alpha = 0.5$ rad, 0.1 rad respectively and $\Delta = 0.999$. It will be seen that the value of the critical Reynolds number does not change once M is greater than 12. The value $M = 12$ was therefore used for the calculations.

Obviously the critical Reynolds number depends on the parameter Δ. As discussed in the introduction, it is more natural to consider Jeffery–Hamel flow in an infinite channel than in the finite one used here. For this reason, we mostly consider the limit $r_2/r_1 \to \infty$ or equivalently $\Delta \to 1$, a limit which we approach by taking Δ very close to 1. However, when Δ is smaller, there can be more than one branch of the neutral curve, as shown in figure 4 for $\Delta = 0.9$. In this case there are multiple regions of instability; however, we found that this behaviour did not occur when $\Delta = 0.999$, the value we have mainly used.

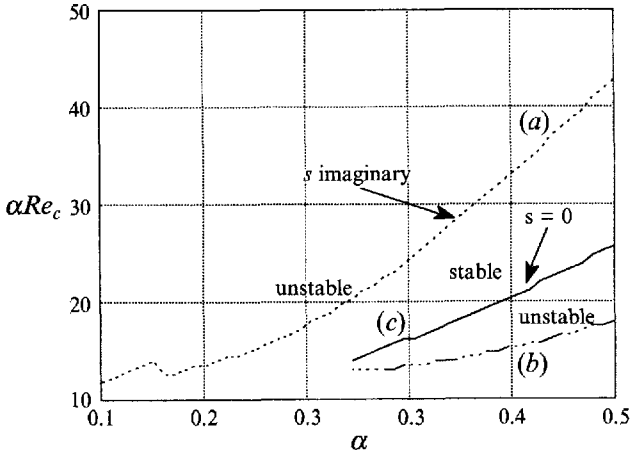

FIGURE 4. A plot of the critical Reynolds number Re_c in the plane (Re_c, α) for $\Delta = 0.9$. There are two branches labelled (*a*) and (*b*)/(*c*). Zero boundary conditions.

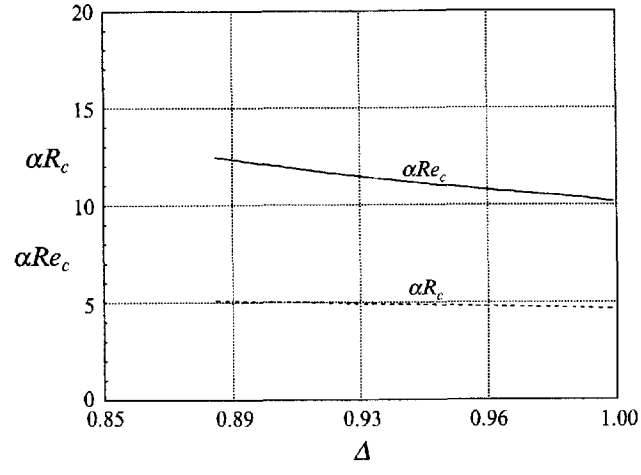

FIGURE 5. The critical Reynolds numbers Re_c and R_c as functions of Δ for $\alpha = 0.1$ rad, zero boundary conditions.

Figure 5 shows the critical Reynolds number as a function of Δ near 1 and indicates that a limit is approached as $\Delta \to 1$ for $\alpha = 0.1$ rad. The product αRe_c decreases slowly with increasing Δ, while the product αR_c is very nearly constant. Unfortunately taking Δ greater then 0.999 introduces a significant numerical error.

Figure 6 shows typical streamlines which result from summing the velocity fields of the basic flow and growing perturbation given by linear theory. The perturbation amplitude is, of course, not fixed by linear theory, and the mode grows exponentially with time. The amplitude was chosen so that the effect of the perturbation was significant but not dominant. Strictly speaking, nonlinear theory should be used for such a large perturbation amplitude (a topic we take up in §5); however, similar patterns to those shown in figure 6 were observed both experimentally and numerically by Sobey & Drazin (1986) in divergent channels with curved walls. Note that an important effect of these patterns is that the flow section is restricted and diverted by the presence of vortices and the flow deceleration is consequently less than for the basic flow alone.

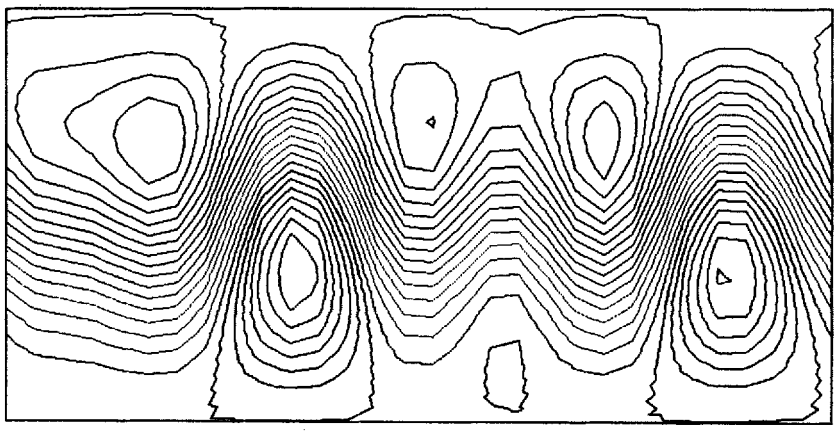

FIGURE 6. The sum of the basic flow and the growing mode according to linear theory – the mode amplitude is arbitrary. $\alpha = 0.1$ rad, $\Delta = 0.999$.

4.4. *Qualitative discussion of some experimental results*

If the patterns of flow described above persisted to large Reynolds number, it might explain the fall in performance of diffusers established experimentally by Carlson, Johnston & Sagi (1967) and Reneau, Johnston & Klim (1967), a point we now elaborate.

Let the pressure coefficient be $C_p = (P_2 - P_1)/(\frac{1}{2}\rho U^2)$, where P_2, P_1 are the pressure at the outlet and inlet sections respectively and U is the inlet velocity based on the volume flux. Carlson *et al.* (1967) showed experimentally using five different values of α that the pressure coefficient takes its greatest value when $\alpha = 0.091$ rad. The same result was obtained by Reneau *et al.* (1967). In Table 2 we give the characteristics of five diffusers used by Carlson *et al.* (1967) and Reneau *et al.* (1967) and the critical Reynolds number for each diffuser according to the present analysis.

Given ideal irrotational flow of an inviscid fluid, the pressure coefficient of a diffuser would increase with α. However, the real flow is not ideal and the coefficient was found to initially increase as α was increased from 0, then decrease again. Viscosity leads to energy loses, but more importantly the flow can separate from the walls of the diffuser leading to a drop in efficiency. Separation is accompanied by recirculation zones near the walls and we believe that the vortex structures apparent in figure 6 (and the corresponding non-linear results, figures 8 and 10, which we will discuss in the next section) are low-Reynolds-number precursors of separation.

Classical laminar boundary layer theory (as described in, for instance, White 1974) for a Falkner–Skan profile predicts separation when the angle α exceeds $\alpha_\sigma = -\frac{1}{2}\beta\pi$, where $\beta = -0.199$, leading to $\alpha_s = 0.312$ rad. This is considerably larger than the value of α at which the diffuser efficiencies are observed to decrease. Furthermore, the laminar boundary layer thickness for such small angles can be estimated using the value $\delta^*/r = O((Re_r)^{-\frac{1}{2}})$. The thickness calculated in this way is much too small to explain the observed loss of efficiency. Turbulent boundary layers tend to be even less susceptible to separation. In summary, classical results for separation seem inadequate to account for the drop in pressure coefficient.

We suggest that separation in diffusers and their consequent loss of efficiency may be due to an instability of the whole flow of the type considered in this paper, with the resulting vortices being the manifestation of separation. Of course, the present study does not extend to the very high Reynolds numbers of the experiments.

We should also mention work by Rodrigues (1990) who used a finite element method

α (rad)	C_p Carlson *et al.*	C_p Reneau *et al.*	C_p Ideal	R_c	Re_c
0.066	0.58	0.61	0.69	74.2	151.5
0.091	0.62	0.65	0.77	53.8	110.9
0.116	0.59	0.63	0.82	42.2	87.7
0.14	0.55	0.60	0.86	35	73.1
0.165	0.50	0.53	0.88	29.6	62.3

TABLE 2. Characteristics of diffusers used by Carlson *et al.* (1978), and Reneau *et al.* (1967). C_p is the pressure coefficient, R_c the critical Reynolds number based on volume flux and Re_c the critical Reynolds number based on the axial velocity.

with boundary conditions derived from several wall turbulence models to compute the pressure coefficient. Good agreement with experiment was found using Meller's law and Nakayama's law, but the logarithmic law failed.

5. Nonlinear analysis

Our aim here is on the one hand to understand the nature of the instability when its amplitude has grown beyond the linear range, and on the other hand to study the interaction between stable and unstable modes. To this end we keep nonlinear terms and derive the nonlinear equivalent of the perturbation equation (2.5). Since we are now concerned with nonlinear equations, for which the absolute magnitude of ψ' is significant, it is convenient to define a non-dimensional perturbation by

$$\psi'_{\text{non-dim}} = \psi'_{\text{phys}}/G(0). \tag{5.1}$$

The resulting equation is

$$\frac{\partial(\nabla^2\psi')}{\partial\tau} + \mathrm{L}(\psi') = \mathrm{N}(\psi', \psi'), \tag{5.2}$$

where $\mathrm{L}(\psi')$ is that part of the linear operator that does not involve time:

$$\mathrm{L}(\psi') = \frac{RG_y}{\alpha\rho}\frac{\partial(\nabla^2\psi')}{\partial\rho} - \frac{2RG_{yy}}{\alpha^3\rho^4}\frac{\partial\psi'}{\partial y} - \frac{RG_{yyy}}{\alpha^3\rho^3}\frac{\partial\psi'}{\partial\rho} - \nabla^4\psi'. \tag{5.3}$$

and $\mathrm{N}(\psi', \psi)$ is the nonlinear part, whose detailed form we do not give here owing to its length. The perturbation stream function ψ' is expanded as follows:

$$\psi' = \sum_{i=1}^{N} A_i(\tau)\,\phi_i(y, \rho), \tag{5.4}$$

where the functions ϕ_i are the eigenfunctions of the linear problem (3.6) (both symmetric and antisymmetric with respect to y). Eigenfunctions satisfying either zero or periodic boundary conditions may be used. For further reference when discussing the results it is convenient to normalize the ϕ_i by requiring $(\phi_i, \phi_i) = 1$, where

$$(\boldsymbol{\phi}, \boldsymbol{\chi}) = \int_{-1}^{1} \mathrm{d}y \int_{-1}^{1} (\boldsymbol{\phi}^*, \boldsymbol{\chi})\,\mathrm{d}\rho \tag{5.5}$$

is a scalar product.

After scalar multiplication of (5.2) by the adjoint eigenfunctions ϕ_i^A and using the fact that they are orthogonal to $\nabla^2\phi_i$, we obtain the following system:

$$\left(\frac{\mathrm{d}A_i}{\mathrm{d}\tau} - s_i A_i\right)(\nabla^2\phi_i, \phi_i^A) = \sum_{m=1}^{N}\sum_{j=1}^{N} A_m A_j (N(\phi_m, \phi_j), \phi_i^A), \quad i = 1, \ldots, N, \tag{5.6}$$

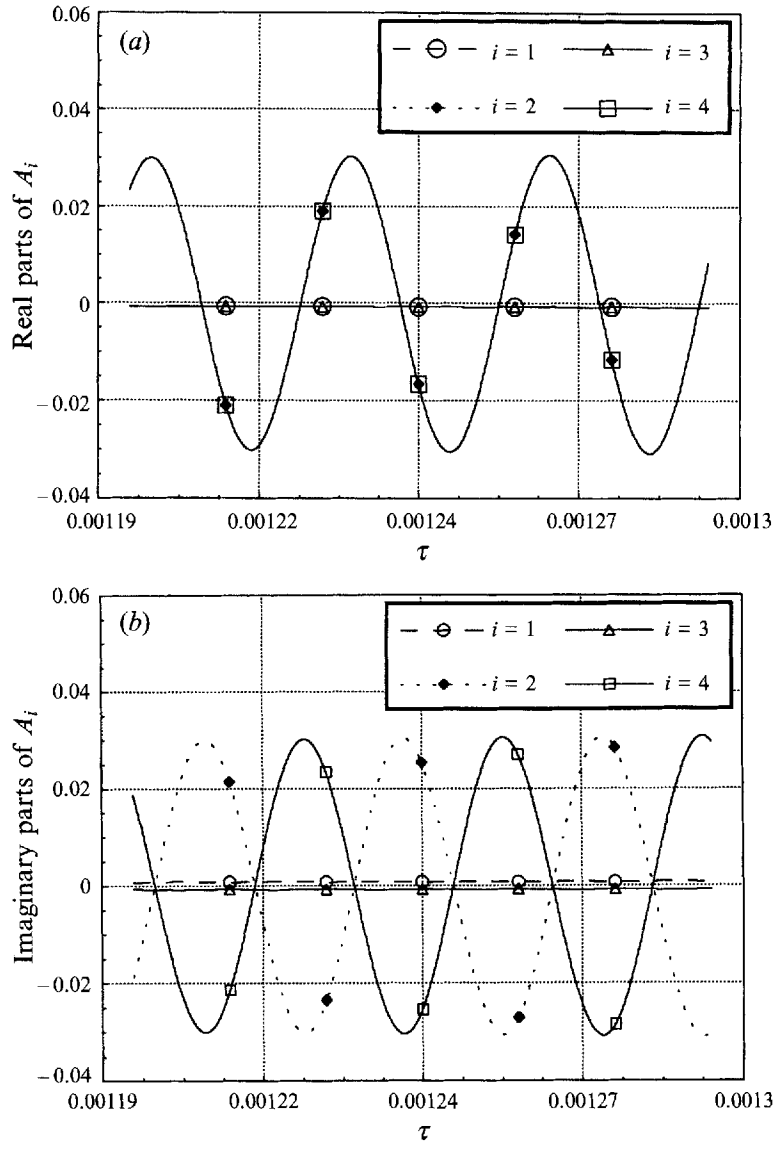

FIGURE 7. The amplitudes A_i as a function of viscous time τ for $\alpha = 0.1$ rad and $\Delta = 0.999$, using periodic boundary conditions: (*a*) real parts of A_i, (*b*) imaginary parts of A_i.

where s_i is the eigenvalue of the linear system (3.6)–(3.8) corresponding to the eigenfunction ϕ_i. For future reference when we come to describe the results, the modes are numbered as follows. Modes for which ϕ_i is antisymmetric with respect to y are labelled $1, 3, 5, \ldots$, while those which are symmetric in y are labelled $2, 4, 6, \ldots$. Modes of a given symmetry are in decreasing order of $Re(s)$, i.e. the most rapidly growing or least rapidly decaying come first. Modes for which s is not real occur twice as a complex-conjugate pair and therefore both modes of the pair have the same value of $Re(s)$. Which of the pair comes first in the ordering is left arbitrary.

The solution of (5.6) depends on α, Δ, Re and the initial conditions. Equation (5.6) was solved by a fourth-order Runge–Kutta method. For Reynolds numbers slightly smaller than the critical value of linear theory, the disturbance was found to approach

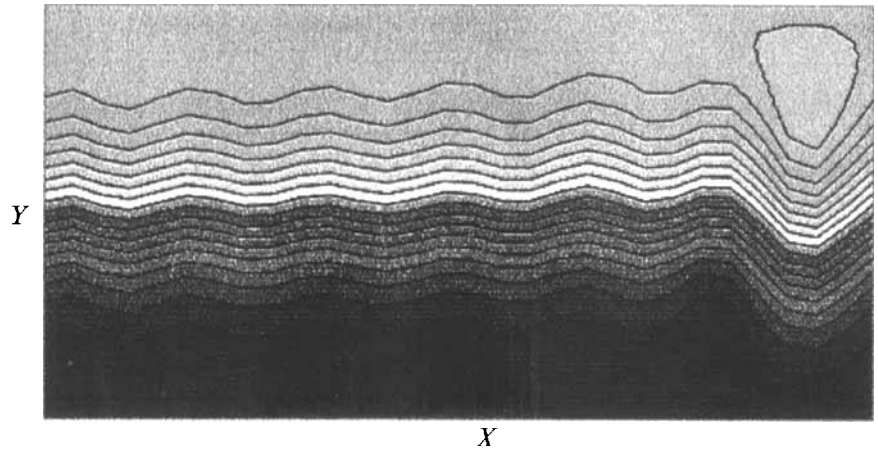

FIGURE 8. The stream function in a divergent channel. Nonlinear solution using periodic boundary conditions: $\alpha = 0.1$ rad and $\Delta = 0.999$ at $\tau = 0.004$.

zero for all initial conditions we tried (with zero boundary conditions, $\alpha = 0.3$, $\Delta = 0.999$ and $N = 20$). This strongly suggests that the flow is globally stable for $Re < Re_c$ and that the critical Reynolds number gives a supercritical bifurcation. The contrast with plane Poiseuille flow (for which the onset of instability is subcritical) is striking. The change in the nature of the instability is no doubt connected with the large reduction in the critical Reynolds number (to about 35 from 5800 for the parameter values quoted above). As α is decreased, the planar result must, of course, be eventually recovered, but as mentioned in the introduction this requires very small values of α, below the range of applicability of the numerical methods used.

When the Reynolds number is slightly greater than its critical value, we expect equilibration of the perturbation amplitude for a supercritical bifurcation. This is indeed what we find:

Case 1

For $\alpha = 0.1$ rad, $\Delta = 0.999$ and periodic boundary conditions the critical Reynolds number is $Re_c = 111.4$, at which growing linear modes appear, while for $Re = 140$ there are two conjugate pair of symmetric growing modes. We take $N = 8$ in (5.6), and consider the four growing symmetric modes together with four antisymmetric modes which are chosen to be the least rapidly decaying according to linear theory. The initial conditions were that the amplitude of the most rapidly growing symmetric mode and its conjugate be $A_2 = A_4^* = 0.001\,(1+i)$ and that all other modes have zero amplitude. The time step is adjusted at each stage according to the amplitude of the perturbation. Thus we choose

$$(\Delta\tau)_n = (\Delta\tau)_0 \Big/ \left[10\left(\sum_{i=1}^{N} |A_i|^2\right)^{\frac{1}{2}}\right], \tag{5.7}$$

where the A_i are the values at the preceding step and $(\Delta\tau)_0 = 10^{-10}$. We found that the solution approached a periodic limit cycle whose form is shown in figures 7(*a*) and 7*b*), which give the A_i as a function of τ. Increasing the number of modes to $N = 12$ did not change these results noticeably.

In figures 7(*a*) and 7(*b*) it can be seen that the symmetric growing mode ($i = 2$) is dominant as we might expect from weakly nonlinear theory close to criticality. Figure 8 shows the streamlines of the flow at one instant of the quasi limit cycle. The term

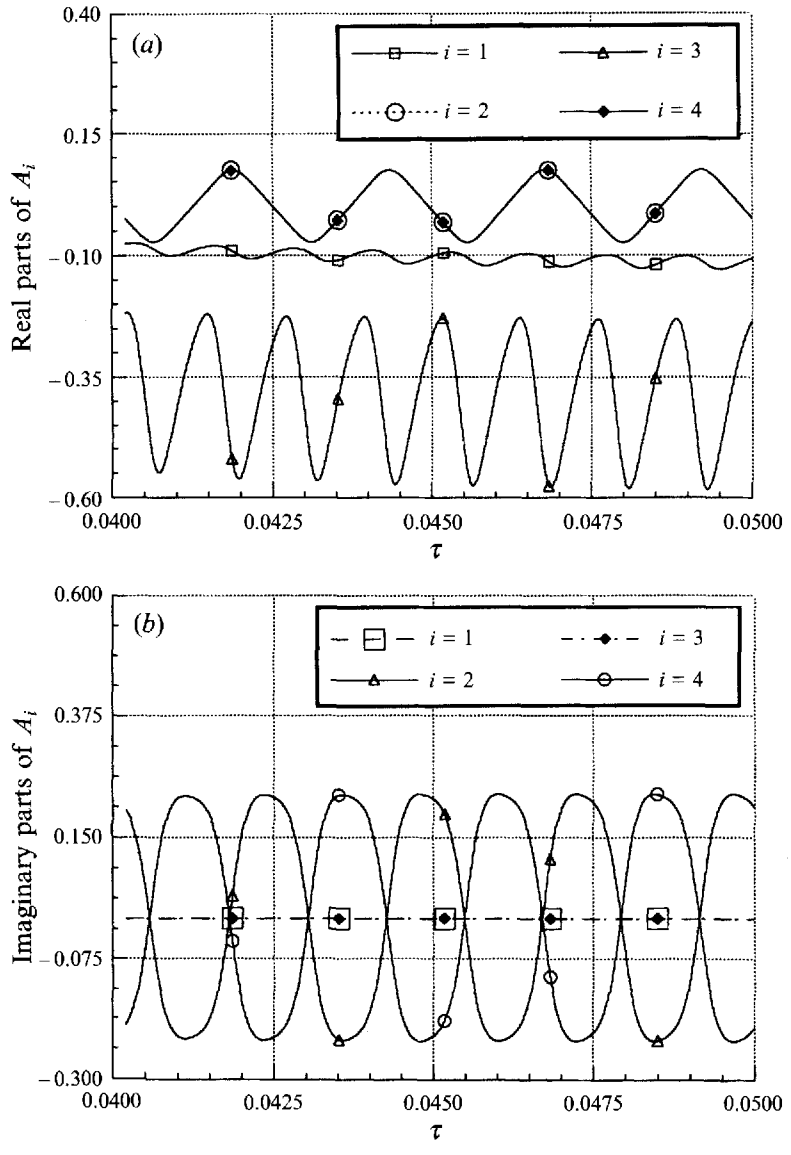

FIGURE 9. The amplitudes A_i as a function of viscous time τ for $\alpha = 0.3$ rad and $\Delta = 0.999$, using zero boundary conditions: (*a*) real parts of A_i, (*b*) imaginary parts of A_i.

quasi-periodic was used above because, in addition to the oscillations shown in figures 7(*a*) and 7(*b*) we also found slower modulations of the modal amplitudes. The timescale for these modulations was of the same order of magnitude as the time required for the basic flow to go the length of the channel. The spatially periodic boundary conditions may be the cause of these temporal modulations, a disturbance which runs the length of the channel being reinjected at the inlet.

Case 2

In this example $\alpha = 0.3$ rad and $\Delta = 0.99$ giving a critical Reynolds number of $Re_c = 35.2$. For $Re = 40$ and using zero boundary conditions, the linear problem has a conjugate pair of symmetric growing modes. We again consider the interaction

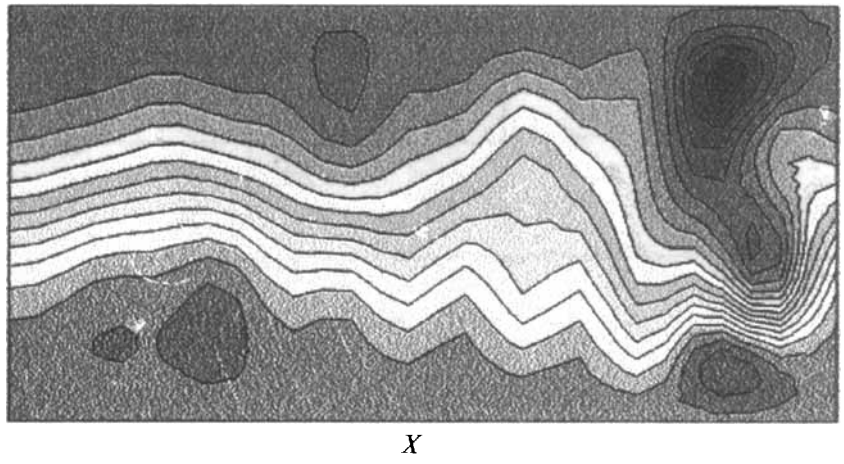

FIGURE 10. The stream function in a divergent channel. Nonlinear solution using zero boundary conditions; $\alpha = 0.3$ rad and $\Delta = 0.999$ at $\tau = 0.05$.

between eight modes which include the two growing as well as the two least rapidly decaying symmetric modes and the four least rapidly decaying antisymmetric modes. The initial amplitude of the single least rapidly decaying symmetric mode is $A_6 = 0.001$ whereas all the others are zero. The step time is adjusted as described above, with $(\Delta\tau)_0 = 10^{-8}$. Increasing the number of modes to $N = 12$ did not lead to noticeable changes.

Figures 9(*a*) and 9(*b*) show the A_i $(i = 1, \ldots, 4)$ as a function of τ for the resulting strictly periodic limit cycle. Perhaps surprisingly the amplitudes of the growing modes are of the same order of magnitude and smaller than those of the decaying modes. Note that for the zero boundary conditions we found no slow aperiodic modulations.

Figure 10 shows the streamlines at one instant of the limit cycle. The pattern is somewhat similar to that shown in figure 8 but there are fewer vortices.

6. Conclusions

The temporal instability of symmetric Jeffery–Hamel flow in a divergent channel with a source located at the apex of the wedge has been treated. It was found that the critical Reynolds number depends on the length of channel, which is represented by the non-dimensional parameter Δ. For $\Delta = 0.9$ we found multiple regions of instability in the (Re, α)-plane, where Re is the Reynolds number based on the axial velocity and α is the half-angle of the channel (see figure 4). These regions disappeared when $\Delta = 0.999$ as shown by figures 1(*a*) and 2(*a*).

It has been shown that the critical Reynolds number based on the axial velocity, Re_c, and that based on the volume flux, R_c, decrease very rapidly with the increasing α and that both αRe_c and αR_c are very nearly linear function of α as shown in figures 1(*b*) and 2(*b*). From the neutral curves we deduce that Jeffery–Hamel flows of types I and II_1 are stable, while flows of type II_2 are unstable.

The neutral curves obtained by the present method for $\Delta = 0.999$ are in good agreement with the result of Sobey & Drazin (1986) using the model of Hooper *et al.* (1982), while they are in disagreement with the Eagles' (1966) results for small α.

The somewhat limited number of cases for which we were able to carry out nonlinear calculations (owing to constrained computed resources) suggest that the critical

bifurcation is supercritical. When the Reynolds number was greater than the critical value an asymmetric, time-periodic or quasi-periodic solution appeared. These oscillatory solutions are interpreted as precursors of flow separation and may explain the drop in the efficiency of diffusers established by experiment.

It is interesting to observe that Sobey & Drazin (1986) found the critical bifurcation to be subcritical, in disagreement with the result obtained here. It should however be borne in mind that their analysis was based on a model problem, rather than derived from the Navier–Stokes equations. Indeed, they found that a numerical calculation for a channel flow using the latter equations showed a supercritical bifurcation, in agreement with our results. This contrasts with plane Poiseuille flow for which there is a subcritical bifurcation.

Presumably the case of plane Poiseuille flow would result from strict application of the mathematical limit $\alpha \to 0$; however, as described in the introduction, the high value of the critical Reynolds number requires very small values of $\alpha = O(Re_c^{-1})$, which we have been unable to attain using the numerical methods described here. It would be interesting to investigate the way in which the transition from the subcritical bifurcation and large critical Reynolds numbers of plane Poiseuille flow to the supercritical bifurcation with moderate values of the critical Reynolds number found here occurs.

REFERENCES

BANKS, W. H. H., DRAZIN, P. G. & ZATURSKA, M. B. 1988 On perturbation of Jeffery–Hamel flow. *J. Fluid Mech.* **186**, 559–581.

BATCHELOR, G. K. 1977 *An Introduction to Fluid Dynamics.* Cambridge University Press.

BRAMLEY, J. S. & DENNIS, S. C. R. 1982 The calculation of eigenvalues for the stationary perturbation of Poiseuille flow. *J. Comput. Phys.* **47**, 179–198.

CARLSON, J. J., JOHNSTON, J. P. & SAGI, C. J. 1967 Effect of wall shape on flow regimes and performance in straight, two-dimensional diffuser. *Trans. ASME J. Basic Engng* **89**, 151.

DEAN, W. R. 1934 Note on the divergent flow of fluid. *Phil. Mag.* **18**, 749–777.

EAGLES, P. M. 1966 The stability of a family of Jeffery–Hamel solutions for divergent channel flow. *J. Fluid Mech.* **24**, 191–207.

FRAENKEL, L. E. 1962*a* Laminar flow in symmetrical channels with slightly curved walls, I. On the Jeffery–Hamel solution for flow between walls. *Proc. R. Soc. Lond.* A **267**, 119–138.

FRAENKEL, L. E. 1962*b* Laminar flow in symmetrical channels with slightly curved walls, II. An asymptotic series for the stream function. *Proc. R. Soc. Lond.* A **272**, 406–428.

GROSCH, C. E. & SALWEN, H. 1968 The stability of steady and time-dependent plane poiseuille flow. *J. Flow Mech.* **34**, 177–205.

HAMADICHE, M. 1985 Analyse spectrale des mécanismes linéaires des écoulement turbulents inhomogénes. Thesis of Doctorat D'Etat, Université Claude-Bernard Lyon-I.

HAMEL, G. 1916 Spiralförmige Bewegungen zäher Flüssigkeiten. *Jahresbericht Deutsch. Math. Vereingung* **25**, 34–60.

HOOPER, A., DUFFY, B. R. & MOFFATT, H. K. 1982 Flow of fluid of non-uniform viscosity in converging and diverging channels. *J. Fluid Mech.* **117**, 383–304.

JEFFERY, G. 1915 The two-dimensional steady motion of a viscous fluid. *Phil. Mag.* (6) **29**, 455–465.

LIN, C. C. 1945*a* On the stability of two-dimensional parallel flow, Part I. *Q. J. Appl. Maths* **3**, 117–142.

LIN, C. C. 1945*b* On the stability of two-dimensional parallel flow, Part II. *Q. J. Appl. Maths* **3**, 218–234.

MELE, P., MORGANTI, M., DICARLO, A. & TATONE, A. 1981 Laminar to turbulent flow study by means of F.E.M. *Proc. Second Intl Conf., Venice 13–16 July* (ed. C. Taylor & B. A. Schrefler).

ORSZAG, S. A. 1971 Accurate solution of the Orr–Sommerfeld stability equation. *J. Fluid Mech.* **50**, 689–703.

RENEAU, L. R., JOHNSTON, J. P. & KLIM, S. J. 1967 Performance and design of straight, two-dimensional diffusers. *Trans. ASME, J. Basic Engng* **89**, 141.

RODRIGUES, J. L. A. D. F. 1990 Méthode de minimisation adaptée à la technique des élément finis pour la simulation des écoulements turbulents avec conditions aux limites non linéaires de proche paroi. Doctoral thesis: E.C.L. 90-016, Ecole Centrale de Lyon.

SOBEY, I. J. & DRAZIN, P. G. 1986 Bifurcation of two-dimensional channel flow. *J. Fluid Mech.* **171**, 263–287.

THOMAS, L. H. 1953 The stability of plane Poiseuille flow. *Phys. Rev.* **91**, 780–783.

WHITE, F. M. 1974 *Viscous Fluid Flow*. McGraw-Hill.